Proceedings of BS2013:
13th Conference of International Building Performance Simulation Association, Chambéry, France, August 26-28

A TRNSYS MODEL OF A BUILDING HVAC SYSTEM WITH GSHP AND PCM THERMAL ENERGY STORAGE – COMPONENT MODELLING AND VALIDATION

Paul McKenna[1] and Donal P. Finn[1]
[1]School of Mechanical and Materials Engineering, University College Dublin, Ireland

ABSTRACT

This paper describes the development of a simulation model using TRNSYS of a building integrated ground source heat pump with a cold phase change material thermal energy storage unit in a lightweight commercial building located in Marseille, France. The development of the overall system model involved the construction of individual models to simulate various components in the building, including a PCM tank, fan coil units, pumps, an air handling unit and the heat pump. The construction of each of the models is discussed, as well as validation and incorporation of each component into a system model.

INTRODUCTION

Motivation

Energy storage is a focus of many electrical utilities presently. The use of more renewable energy (especially solar and wind energy) can lead to an imbalance between demand and supply. This imbalance can be managed by producing and storing thermal energy when there is excess supply, and using the stored energy when there is high demand. Arce et al. (2011) showed that the use of thermal energy storage (TES) could lead to a potential electrical load reduction in the EU of 7.5% with an expected CO_2 reduction of 5.5%. Ice TES is commonly used in the USA. Braun (2007b) describes a method of charging and discharging an ice TES system that realises savings within 2% of the theoretical maximum possible savings. This leads to savings that can be as high as 60% compared to chiller priority control, with typical savings between 25% and 30% (Braun, 2007a). Chaichana et al. (2001) showed cost reductions of 55% with full ice storage compared to a system without TES.

Ground source heat pumps (GSHPs) have an established market in Scandanavia, Germany, Austria and Switzerland. For example, in Sweden, 18% of heating systems in family homes are GSHPs (Forsén and Nowak, 2010). More recently, there is evidence of strong growth of this sector in several other European markets, especially the UK and France (Forsén and Nowak, 2010). Although the use of GSHPs is increasing in northern France, it is still less common for them to be used in southern France or indeed other Mediterranean climates. GSHPs have been shown to offer many advantages compared to other space conditioning systems. Approximately 1.4% of residential heating in Europe is provided by GSHPs, saving around 0.7% of greenhouse gas emissions compared to a traditional heat mix defined as 50% gas, 30% oil, 10% solid fuel and 10% electricity (Bayer et al., 2012). Blum et al. (2011) calculated that one GSHP can reduce the yearly CO_2 emissions of an average person by 20%. There are drawbacks to the installation of GSHPs, including high capital costs and invasive installation procedure as well as underperformance of heat pumps due to incorrect system design (Boait et al., 2011). Despite the high capital cost, Bolling and Mathias (2008) showed GHSPs to have the shortest payback compared to three other heating and cooling systems in five different US cities. The other systems studied were: a high efficiency furnace and electric air conditioner; an absorption air conditioner and direct electrical heating; and a thermally driven heat pump. This shows the advantage of GSHPs over other technologies in situations where heating and cooling loads co-exist.

The two technologies mentioned above – GSHPs and TES – deal with the electricity storage issue, and the need for efficient combined heating and cooling technologies. However, there is little research in the literature into integrated GSHP and TES systems or into the optimisation of such a system. This highlights a need for the study of integration and optimisation issues relating to these systems.

The objective of the current paper is to describe the construction and validation/calibration of the component models needed to create a model of a building, with a GSHP, phase change material (PCM) TES and other components. The individual component models need to be as accurate as possible over the full range of operating conditions to allow for future development of system operational optimisation algorithms and controls.

Literature Review

Latent heat TES has many advantages over sensible energy storage including: a small temperature operating range, a low input temperature (for heat storage) and a lower weight per unit storage capacity (Abhat, 1981). Numerical models for PCM TES in a packed bed of spherical capsules have been formulated by numerous researchers. Many of these models are based on the enthalpy method (Voller, 1987) and model the PCM as a lumped capacitance system. They have also included effects such as subcooling (Bédécarrats et al.,

2009b), internal resistance (Regin et al., 2009), axial convection (Beasley and Clark, 1984), hysteresis (Bony and Citherlet, 2007).

There are various methods to model cooling (and heating) coils. The coils are effectively cross flow heat exchangers and the equations for such systems are well defined. The problem becomes more complex when there is dehumidification involved. Techniques for solving wet-coil heat transfer are mentioned by Stoecker and Jones (1982) and ASHRAE (2008).

For many heat pump models, dynamic phenomena are neglected. There are two main ways of modelling heat pumps – one common way is to use a correlation from manufacturers catalogue data or a curve-fit model, as seen in Albieri et al. (2009), while the second is to construct a heat pump model from basic thermodynamic equations, as used by Badescu (2002); Chargui et al. (2012). Curve-fit models are usually less accurate over a wide range of operating conditions, while thermodynamic models require detailed knowledge of the individual heat pump components.

BUILDING DESCRIPTION

The building that is being modelled as part of this research is a commercial building with office space of 250 m^2 and a workshop with an area of 88 m^2. A schematic representation of the building can be seen in Figure 1.

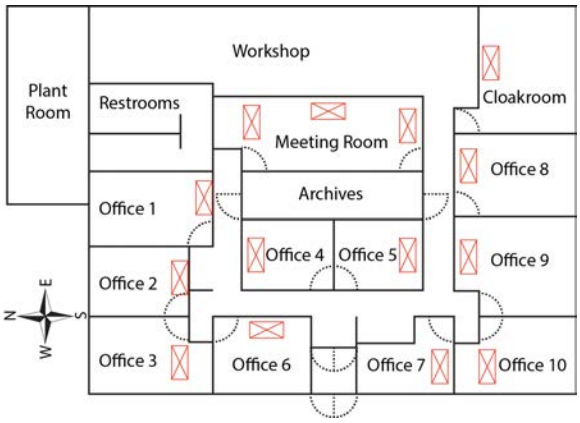

Figure 1: Plan view of the building being modelled with FCU location.

The building is located close to Marseille in the south of France. The design temperature in Marseille for heating is -1.3 °C while for cooling it is 30.9 °C (ASHRAE, 2005). The building is heated and cooled using a tandem compressor GSHP with a capacity of 26.3 kW in heating mode and a capacity of 25.9 kW in cooling mode. Considering Figure 2, the building loop consists of two decoupled networks; the primary network consisting of the heat pump, a buffer tank and a decoupling tank while the secondary network is fed from the decoupling tank and includes the Fan Coil Units (FCUs) which heat/cool the individual rooms.

There is a second circuit that consists of a small heat pump with 4.2 kW cooling capacity. This heat pump is used to supply cooling to a tank containing encapsulated PCM with a melting temperature of 0 °C. This PCM is then used to supply cooling and dehumidification to an air handling unit (AHU) during the summer.

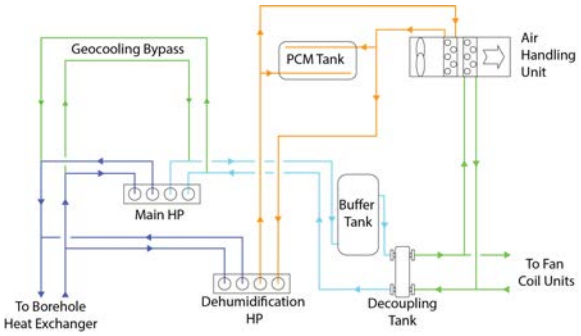

Figure 2: Hydronic circuit.

COMPONENT MODELLING AND CALIBRATION/VALIDATION

PCM Tank

The installed PCM tank is cylindrical, with a volume of 0.5 m^3. It is filled with capsules of 98 mm diameter that are moulded from a blend of polyolefins and filled with a PCM with a melting temperature of 0 °C.

The PCM tank model is a modified version of a numerical analysis published by Regin et al. (2009). This numerical analysis has the following assumptions:

- There is no radial variation of temperature or flow.
- There are no heat losses from the tank.
- The tank is split into N nodes, each of which has uniform heat transfer fluid and PCM temperatures.
- Specific heats and other fluid properties are constant with temperature.
- There is no internal heat generation and no radiant heat transfer.

An energy balance on a section of the tank with length $\mathrm{d}x$ (Figure 3) can be seen in Equation 1.

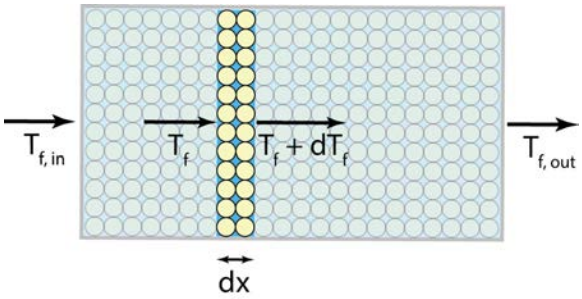

Figure 3: Representation of tank with element of length $\mathrm{d}x$.

$$\dot{m}_f c_{p,f} \left(T_f + \mathrm{d}T_f\right) - \dot{m}_f c_{p,f} T_f + U A_l \left(T_b - T_f\right) \mathrm{d}x = 0 \qquad (1)$$

Where A_l is the surface area of the capsules per unit length. This equation is rearranged as:

$$\frac{\mathrm{d}T}{\mathrm{d}x} = \frac{UA_l}{\dot{m}_f c_{p,f}} \left(T_f - T_b\right) \quad (2)$$

Integration of this equation over a finite control volume, i of length l/N yields:

$$T_{fi+1} = T_{bi} + \left(T_{fi} - T_{bi}\right) \exp\left(\frac{UA_s}{\dot{m}_f c_{pf}}\right) \quad (3)$$

Using this equation, the outlet temperature from a node can be calculated if the inlet temperature of the heat transfer fluid (HTF) and the temperature of the PCM capsules are known.
The enthalpy change of the bed over a time-step Δt can be written as:

$$\left(h_{bi}^{n+i} - h_{bi}^{n}\right) \rho_b \left(1 - \varepsilon\right) Al = \left(UA_s\right) \Delta t \left(T_{fi}^{n} - T_{bi}^{n}\right) \quad (4)$$

From this equation, the change in enthalpy of the PCM for the next time-step can be calculated. To calculate the temperature of the PCM, the melting point of the PCM is assumed to occur over a finite temperature range, $T_{m,l}$ to $T_{m,h}$. The latent heat of fusion is spread linearly over this temperature range. This can be seen in Figure 4.

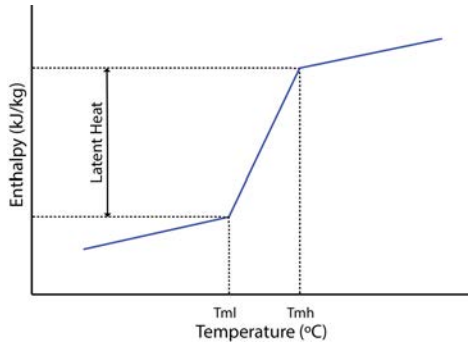

Figure 4: Latent heat of PCM spread over a finite temperature difference

It was required that this model would be as computationally simple as possible. Therefore it was decided not to include an internal resistance model. The absence of such an internal PCM resistance model necessitated the addition of a compensation factor to the HTF Nusselt number, so that the calculated rate of heat transfer to/from the PCM was correct.
The approach outlined by Regin et al. (2009) was not validated, therefore it was decided to use results found in the literature for validation and calibration. Experimental results published by Bédécarrats et al. (2009a) were used as they were from a similar setup to the installed tank. The tank had a volume of 1 m^3 compared to 0.5 m^3 while the PCM had the same melting temperature and was encapsulated in spheres of a similar diameter – 77 mm compared to 98 mm. The heat transfer fluid for both was a mixture of glycol and water and the experiments were performed at temperatures and flow rates similar to the design conditions for the installed system. Comparisons against the results published by Bédécarrats et al. (2009a) can be seen in Figures 5, 6, 7 and 8. In these figures, the experimental results published by Bédécarrats can be seen in black, while simulated results are coloured.
Figure 5 shows that the inlet temperature of the HTF can have a large impact on the time it takes the tank to charge fully. A reduction in the temperature of 2.3°C from -3.8°C to -6.1°C has the effect of almost halving the charging time.

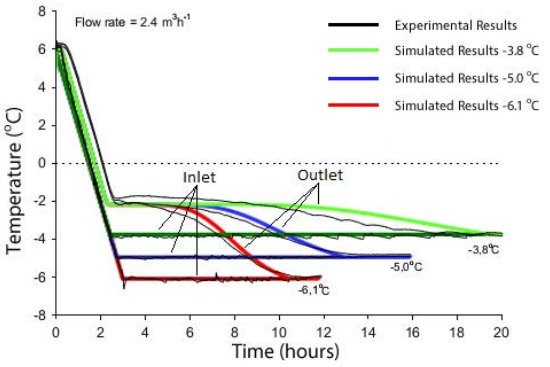

Figure 5: Tank Charging - Comparison of outlet temperatures for 3 inlet temperatures: -3.8 °C (green), -5 °C (blue) and -6.1 °C (red). After Bédécarrats et al. (2009a).

In Figure 6, the effect of an increasing HTF flowrate can clearly be seen, decreasing the time taken to fully charge the tank from 18 hours to 11 hours as the flow rate increases from 1.1 m^3/h to 2.5 m^3/h.

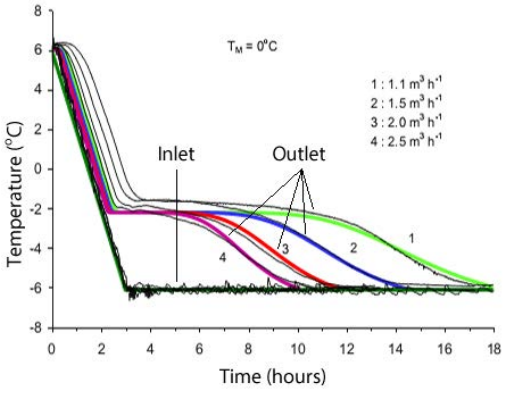

Figure 6: Tank Charging - Comparison of predicted outlet temperatures and charging times for different HTF flow rates. $T_{\mathrm{inlet}} - 6.2°C$ After Bédécarrats et al. (2009a).

Figures 7 and 8 show plots for the discharging of the PCM tank. These figures show less error than those for charging of the TES tank as there is less complexity inherent in the discharging process. This is due to the combined effect of the lack of PCM subcooling, coupled with a reduced internal PCM resistance as the liquid outer layer on melting has a lower ther-

mal resistance than the solid layer when charging due to convection.

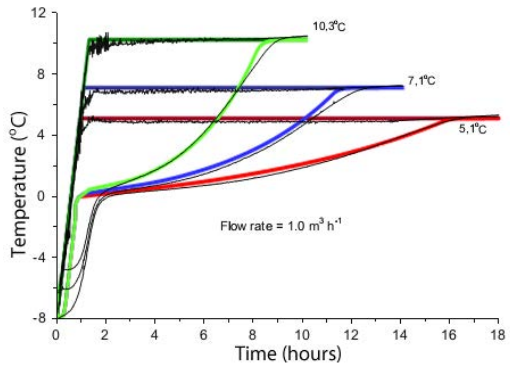

Figure 7: Tank Discharging - Comparison of outlet temperatures for 3 inlet temperatures: 10.3 °C (green), 7.1 °C (blue) and 5.1 °C (red). After Bédécarrats et al. (2009a).

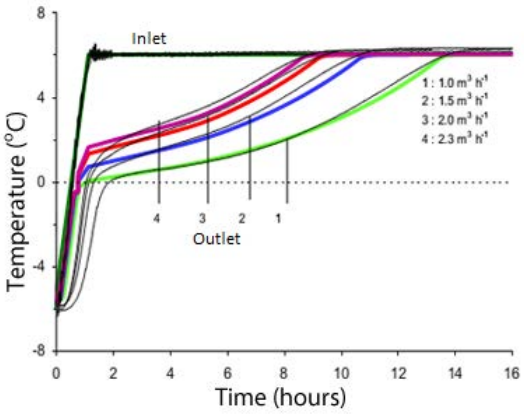

Figure 8: Tank Discharging - Comparison of predicted outlet temperature for different HTF flow rates. After Bédécarrats et al. (2009a).

Good agreement with experimental values is shown in all cases, with slightly more error for cooling than heating. The maximum error in simulated outlet temperature under steady state conditions is 0.64 °C, while the total simulated charging time of the tank has a maximum error of 10.6%. At a steady inlet temperature, the RMS error in outlet temperature for a full charging or discharging cycle varies between 0.15 °C and 0.37 °C for the different inlet conditions, with an average value of 0.24 °C for heating and 0.27 °C for cooling.

Fan Coil Units

The FCUs were modelled using a correlation from software provided by their manufacturer. The original software was used to calculate the sizing of units for customers. Using this software, a table of data for various operating points was established.
Using this table, a correlation for the UA value of the heat exchanger was established in the following format:

$$UA = c_1\dot{m}_{air} + c_2\dot{m}_{water} + c_3\dot{m}_{air}\dot{m}_{water} + c_4 \quad (5)$$

The heat transfer in the FCU was then calculated using the NTU-effectiveness method, where the effectiveness, ε, is defined in Equation 6 for a cross flow heat exchanger with both fluids unmixed.

$$\varepsilon = 1 - \exp\left(\frac{NTU^{0.22}}{C_r}\left(\exp\left(-C_r NTU^{0.78}\right) - 1\right)\right) \quad (6)$$

Where NTU is the number of transfer units $= UA/C_{min}$. C_{min} is the lower heat capacity rate, while C_r is the ratio of C_{min} to C_{max}. The heat transfer and outlet temperatures from the FCU can then be calculated.
The UA value for a heat exchanger is a function of the heat exchanger itself and the flow rate of the air and water through the heat exchanger. As the UA value for the heat exchanger is independent of the temperature of the two fluids, this correlation for the UA value of the heat exchanger was calculated using values of the FCU in heating mode, with an inlet water temperature of 40°C.
The fan power of the FCUs and the pressure drop of the water through the FCU were calculated similarly, with the power being a function of air flow rate and the water pressure drop being a function of water flow rate:

$$P_{fan} = e_1\dot{m}_{air}^2 + e_2\dot{m}_{air} + e_3 \quad (7)$$

$$\Delta P = d_1\dot{m}_{water}^2 + d_2\dot{m}_{water} + d_3 \quad (8)$$

A plot of the UA value against air and water flowrate can be seen in Figure 9. The average error between the correlation and the data points is 3.5%. The accuracy of the model could have been improved slightly by adding $\dot{m}^2$ terms to Equation 5, but as the error is low, it was decided to leave it as it is for computational simplicity.

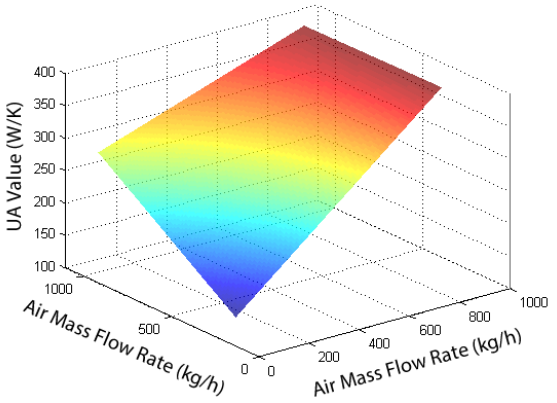

Figure 9: FCU UA Correlation with Mass Flow Rate for Heating

A separate model using the same technique was used for cooling, with a piecewise linear method used to

calculate the fan coil heat transfer with latent behaviour under dehumidification conditions. This can be seen in Figure 10.

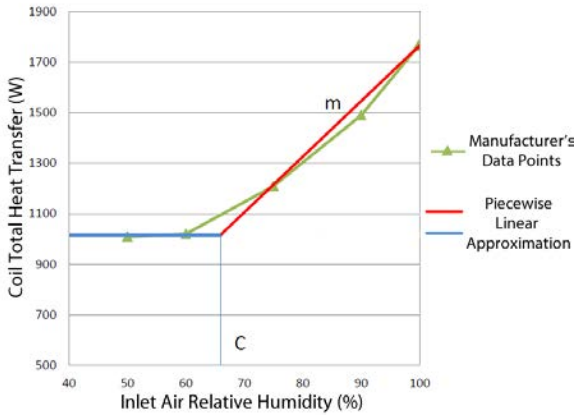

Figure 10: FCU piecewise linear approximation fitted to manufacturer's data points.

This method assumes that the heat transfer in the FCU remains constant below a certain humidity, marked as "C" in Figure 10, and then increases linearly, with slope m.
It was further assumed that for the narrow temperature operating range of the FCU (approximately 20 – 25 °C), C and m are only dependent on the constant heat transfer rate that occurs at lower humidity. A plot of heat transfer against inlet humidity ratio for various air and water temperatures can be seen in Figure 11.

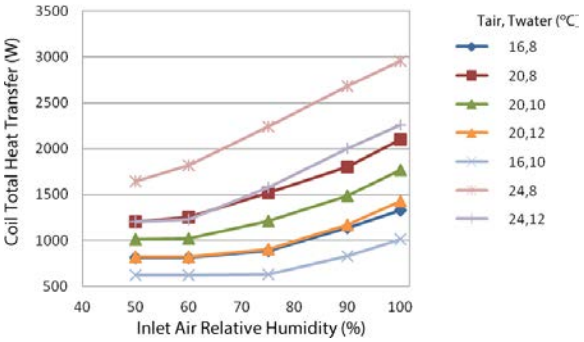

Figure 11: FCU heat transfer for varying humidity.

To calculate the outlet temperature, it was assumed that the cooling of the air would follow an idealised cooling with dehumidification curve. This curve assumes a uniform air temperature as it passes over the coil. The heat transfer for various humidities is calculated with an average error of less than 5.5%.

Air Handling Unit

As with the FCUs, software from the manufacturer was available to model the coils in the AHU. In the AHU, there are two different coils – one for heating and one for cooling – so different correlations needed to be determined for heating and cooling. The cooling coil is being supplied from the PCM tank and is mainly used for the purpose of dehumidification – the coils are not finned and therefore the sensible heat transfer is low.
The air mass flow rate is constant ($\dot{m}_{air}$ = 600 kg/h), so the heat transfer is dependent on the inlet temperatures of water and air ($T_{in,w}$ and $T_{in,a}$), the relative humidity (RH) and the water mass flow rate ($\dot{m}_{water}$). Because the cooling coil was optimised for dehumidification, the idealised cooling with dehumidification process described previously for the FCUs could not be used in this case, as the assumption that the air would be at a uniform temperature would be invalid. Therefore, a new variable, c_p^*, was defined to be the ratio of the total heat transfer from one kilogram of the air to the change in dry bulb temperature of the air. A correlation for c_p^* was calculated from the manufacturers data. This correlation assumes that the water in the AHU coil is at a constant temperature, which is an acceptable assumption as the temperature difference between the water and the air is quite high (ΔT ranges from approximately 15 to 35 °C).
The correlation was calculated using a regression analysis and the error was calculated for a set of data points representing the operating range of the AHU. This error was calculated to be an average of 3.6%.

Pumps

There are 5 different pumps in the system. Each of them is a variable speed unit, and adjusts it's speed so that a constant pressure across the system is maintained.
The pump correlations were created from the graphs supplied in the manufacturers' data sheets. The description below uses values and data from the Grundfos Magna 25-60 pump but the methods were similar for all of the pumps.
The only data that was available for the pumps were the performance curves from the manufacturer's data sheets (see Figure 12). In order to effectively model the pump, an equation for power in terms of flow rate for the each pressure drop was determined. It was assumed that the curves could be accurately modelled using a quadratic equation (Equation 9).

$$P_h = a_h Q^2 + b_h Q + c_h \tag{9}$$

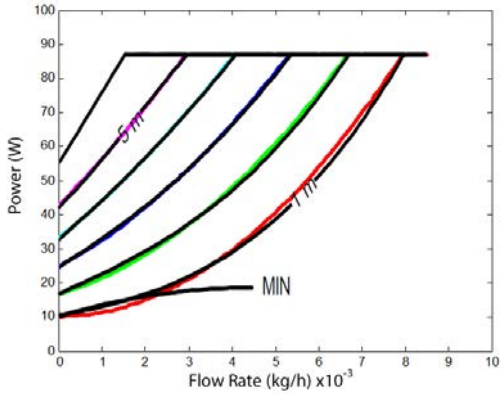

Figure 12: Fitted Curves for Magna 25-60.

When this equation is evaluated for each of the values for head, and superimposed on the original curves, it yields the result shown in Figure 12.
A single expression for power in terms of head was calculated by performing a regression analysis on a_h, b_h and c_h which leads to an equation of the form:

$$P = (a_1 h + a_2)Q^2 + (b_1 h + b_2)Q + (c_1 h + c_2) \quad (10)$$

The coefficients a_1, a_2, b_1, b_2, c_1 and c_2 are found by fitting trend lines to a plot in EXCEL of the coefficients a_h, b_h and c_h. Using these correlations, the overall pump equation becomes:

$$\begin{aligned} P \quad &= (-0.1493h + 1.3468)Q^2 + \quad (11) \\ &(3.3186h - 3.1234)Q + (8.1055h + 1.1927) \end{aligned}$$

Using this correlation to plot the power for the original values of head, the result can be seen in Figure 13.

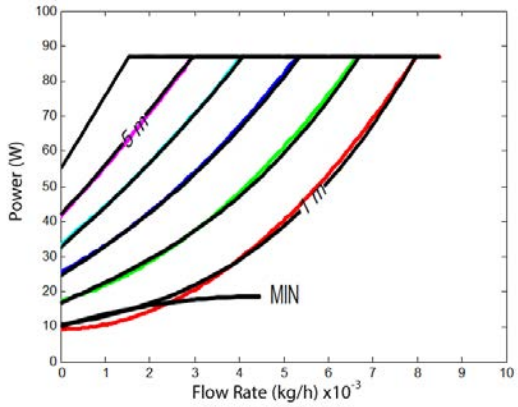

Figure 13: Fitted Curves for Magna 25-60 using correlation.

This correlation will then work at any value for head and flow rate within the range of study. If the calculated power is above 87 W (P_{max}) the power is then set to P_{max}. The correlations for the other pumps were calculated using the same method. As with the first pump where the highest RMS error has been calculated as 1.76 W for a pressure drop of 1 m, the errors are minimal compared with the level of data available.

Ground Source Heat Pump

Data was available from the heat pump manufacturer for over 3000 operating points. This allowed a correlation to be constructed that would cover the full operating range of the heat pump (Equation 12).

$$\begin{aligned} P = c_1\dot{m}_{evap} + c_2\dot{m}_{cond} + c_3T_{evap}^2 + c_4T_{evap} \\ + c_5T_{cond}^2 + c_6T_{cond} + c_7 \quad (12) \end{aligned}$$

Table 1 shows the error for the three correlations described in Equation 12 where the variable P signifies the heat transfer in the evaporator (P_{evap}), the heat transfer in the condenser (P_{cond}) or the electrical power consumed by the compressor (P_{comp}).

Table 1: Error in correlations

	Standard Error (%)
P_{evap} (1 Comp)	1.23
P_{evap} (2 Comps)	1.36
P_{cond} (1 Comp)	0.99
P_{cond} (2 Comps)	1.15
P_{comp} (1 Comp)	0.31
P_{comp} (2 Comps)	0.50

The COP of the heat pump can be seen in Figures 14 and 15.

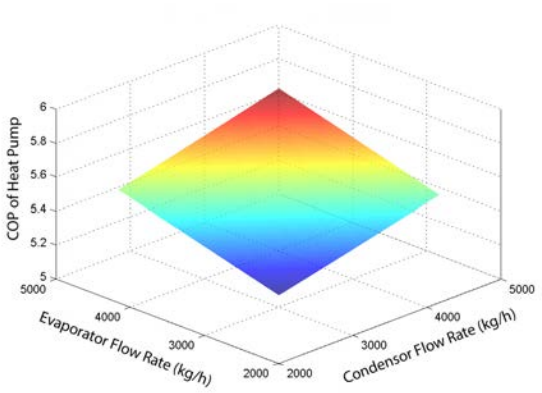

Figure 14: COP of the heat pump at the design temperatures: $T_{cond} = 35\ °C$ and $T_{evap} = 15\ °C$.

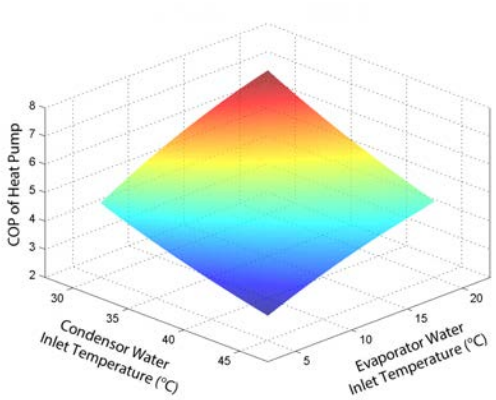

Figure 15: COP of the heat pump at the design flow rates: $\dot{m}_{cond} = 4500$ kg/h and $\dot{m}_{evap} = 3800$ kg/h.

Figure 14 shows how the COP varies at constant inlet temperatures, while Figure 15 shows the COP of the heat pump as a function of the inlet temperature. It can be seen (note the magnified COP axis in Figure 14) that while the mass flow rates through both the evaporator and the condenser have little effect on the COP, the inlet temperature on both sides can have a substantial effect on the COP of the heat pump.

Building Model

The model of the building was created in the TRNSYS plugin for Google SketchUp. The building was

split into 19 thermal zones, with each room being its own zone. An image of the SketchUp model of the building can be seen in Figure 16.

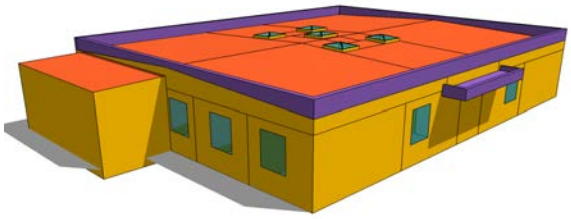

Figure 16: Google SketchUp model of the building.

A calculation of the loads on the building was performed. These loads were calculated zone by zone on an hourly basis. From these values, the total monthly loads were calculated. These can be seen in Figure 17.

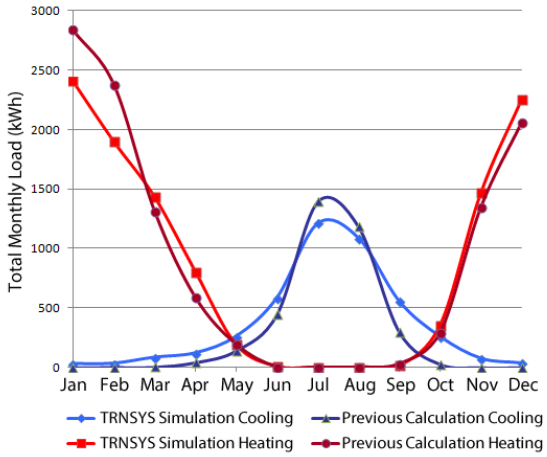

Figure 17: Monthly heating and cooling loads on the building (kWh).

The values in Figure 17 equate to an annual cooling load of 4.4 MWh and heating load of 10.8 MWh, or total annual thermal consumption of 64 kWh/m^2. The equivalent values calculated by the company that owns the building show good agreement at 3.6 MWh, 11.0 MWh and 61 kWh/m^2 respectively.

Incorporation into TRNSYS

The TRNSYS simulation studio has a standard library of components. This can be added to by writing a program in C++ or FORTRAN and compiling it to create a new component. Each component has a predefined number of inputs, parameters and outputs. Inputs are values that will be read at each time-step of a simulation, and are often the outputs of other components. Parameters are values that can be adjusted from simulation to simulation but stay constant for the duration of the simulation. Outputs are values that are calculated during every time-step of a simulation and usually depend on the values of the parameters and inputs. An output of a component can be the input of another component for that time-step.

Each system component described above (PCM tank, GSHP, FCU, AHU and pumps) were programmed as separate TRNSYS components and integrated with the building model to create a complete system model.

CONCLUSION

This paper presents the creation of validated TRNSYS models of an encapsulated PCM TES tank, a tandem compressor GSHP, an FCU, an AHU and a number of pumps. The heat pump, FCU and AHU were validated against data points provided by the manufacturer of the components and all showed reasonable agreement with these values.

The PCM tank was validated against experimental values from the literature and shows a very acceptable level of error. The pumps were compared to the manufacturer's data curves and show little deviation from these plots.

The FCU model used a novel method to calculate the heat transfer in the heat exchanger when there is dehumidification of the air. This involved a computationally simple solution that was relatively accurate over the FCU's limited operating range.

For the AHU, a different solution had to be obtained due to the larger variation in inlet air temperature. This led to the definition of an equivalent heat capacity, which was used to calculate the sensible and latent cooling to an acceptable degree of accuracy.

These validated models are used to form an accurate, yet computationally simple model of a building in a Mediterranean climate with GSHP, and PCM TES.

NOMENCLATURE

Abbreviations

AHU	Air Handling Unit
FCU	Fan Coil Unit
GSHP	Ground Source Heat Pump
HTF	Heat Transfer Fluid
HVAC	Heating, Ventilation and Air-Conditioning
PCM	Phase Change Material
TES	Thermal Energy Storage

Symbols

A	Cross sectional area of tank (m^2)
A_l	Surface area of capsules per unit length of tank (m)
A_s	Surface area of capsules per node (m^2)
c_p	Specific heat capacity (kJ/kgK)
h	Specific enthalpy (kJ/kg)
l	Length of tank (m)
$\dot{m}$	Mass flow rate (kg/h)
N	Number of nodes in tank
P	Power (kW)
q	Rate of heat transfer (kW)
Q	Volumetric flow rate (m^3/hr)
RH	Relative humidity (%)
T	Temperature (°C)
U	Overall heat transfer coefficient (W/m^{2}K)
ε	Voidage fraction of bed or heat exchanger effectiveness
ρ	Density (kg/m^3)

Superscripts and Subscripts

b	PCM bed
comp	compressor
cond	condenser
evap	evaporator
f	heat transfer fluid
i	spatial location in PCM tank
n	temporal stage of simulation

ACKNOWLEDGEMENTS

This research has been supported by the Irish Research Council's Embark Initiative and by the FP7 GroundMed project (DG TREN/FP7EN/218895).

REFERENCES

Abhat, A. 1981. Short term thermal energy storage. *Energy and Buildings*, 3(1):49 – 76.

Albieri, M., Beghi, A., Bodo, C., and Cecchinato, L. 2009. Advanced control systems for single compressor chiller units. *International Journal of Refrigeration*, 32(5):1068 – 1076.

Arce, P., Medrano, M., Gil, A., Oró, E., and Cabeza, L. F. 2011. Overview of thermal energy storage (tes) potential energy savings and climate change mitigation in spain and europe. *Applied Energy*, 88(8):2764 – 2774.

ASHRAE 2005. *ASHRAE Handbook of Fundamentals*. American Society of Heating, Refrigerating and Air-Conditioning Engineers.

ASHRAE 2008. *ASHRAE Handbook of HVAC Systems and Equipment*. American Society of Heating, Refrigerating and Air-Conditioning Engineers.

Badescu, V. 2002. Model of a space heating system integrating a heat pump, photothermal collectors and solar cells. *Renewable Energy*, 27(4):489 – 505.

Bayer, P., Saner, D., Bolay, S., Rybach, L., and Blum, P. 2012. Greenhouse gas emission savings of ground source heat pump systems in europe: A review. *Renewable and Sustainable Energy Reviews*, 16(2):1256 – 1267.

Beasley, D. E. and Clark, J. A. 1984. Transient response of a packed bed for thermal energy storage. *International Journal of Heat and Mass Transfer*, 27(9):1659 – 1669.

Bédécarrats, J., Castaing-Lasvignottes, J., Strub, F., and Dumas, J. 2009a. Study of a phase change energy storage using spherical capsules. part i: Experimental results. *Energy Conversion and Management*, 50(10):2527 – 2536.

Bédécarrats, J., Castaing-Lasvignottes, J., Strub, F., and Dumas, J. 2009b. Study of a phase change energy storage using spherical capsules. part ii: Numerical modelling. *Energy Conversion and Management*, 50(10):2537 – 2546.

Blum, P., Campillo, G., and Klbel, T. 2011. Techno-economic and spatial analysis of vertical ground source heat pump systems in germany. *Energy*, 36(5):3002 – 3011.

Boait, P., Fan, D., and Stafford, A. 2011. Performance and control of domestic ground-source heat pumps in retrofit installations. *Energy and Buildings*, 43(8):1968 – 1976.

Bolling, A. L. and Mathias, J. A. 2008. Investigation of optimal heating and cooling systems in residential buildings. *ASHRAE Transactions*, 114(1):128 – 139.

Bony, J. and Citherlet, S. 2007. Numerical model and experimental validation of heat storage with phase change materials. *Energy and Buildings*, 39(10):1065 – 1072.

Braun, J. E. 2007a. Impact of control on operating costs for cool storage with dynamic electric rates. *ASHRAE Transactions*, 113 (2):343 – 354.

Braun, J. E. 2007b. A near-optimal control strategy for cool storage systems with dynamic electric rates. *HVAC&R Research*, 13 (4):557 – 580.

Chaichana, C., Charters, W. W. S., and Aye, L. 2001. An ice thermal storage computer model. *Applied Thermal Engineering*, 21(17):1769 – 1778.

Chargui, R., Sammouda, H., and Farhat, A. 2012. Geothermal heat pump in heating mode: Modeling and simulation on trnsys. *International Journal of Refrigeration*, 35(7):1824 – 1832.

Forsén, M. and Nowak, T. 2010. *Outlook 2010: European Heat Pump Statistics*. European Heat Pump Association EEIG (EHPA).

Regin, A. F., Solanki, S., and Saini, J. 2009. An analysis of a packed bed latent heat thermal energy storage system using PCM capsules: Numerical investigation. *Renewable Energy*, 34(7):1765 – 1773.

Stoecker, W. and Jones, J. 1982. *Refrigeration and Air Conditioning*. McGraw-Hill series in mechanical engineering. McGraw-Hill.

Voller, V. 1987. An implicit enthalpy solution for phase change problems: with application to a binary alloy solidification. *Applied Mathematical Modelling*, 11(2):110 – 116.